Leadership in Sustainable Infrastructure
Leadership en Infrastructures Durables

Vancouver, Canada
May 31 – June 3, 2017/ *Mai 31 – Juin 3, 2017*

OPTICAL REMOTE SENSING TECHNIQUE FOR THE GENERATION OF MEANDERING RIVER CHANNEL TOPOGRAPHY AND SEDIMENT SIZE

Harada, Sho.[1,4], Li, S. Samuel[2] and Lapointe, Michel[3]
[1] Concordia University, Canada
[2] Concordia University, Canada
[3] McGill University, Canada
[4] shoharada10@gmail.com

Abstract: Traditional cross-section survey techniques are costly, time-consuming, and difficult to implement, particularly in inaccessible areas. Practical limitation in the spacing and frequency of survey points restricts ground-based survey to reach scale. This paper demonstrates the potential of sizing bed materials within complex shallow channels, using high-resolution multispectral and stereo images. The demonstration uses a 13-km long reach of meandering, alluvial river (the Goulais River in Ontario). Fluvial remote sensing provides complimentary alternative to field survey, in which a watershed-scale, synoptic view of the river may be acquired. The presented technique generates a river topography model (RTM) by combining water depth map (bed to free surface) and the dry surface elevation map (free surface and above). The former is generated from the depth-to-brightness ratio that is empirically estimated by correlating available field survey points to the digital numbers of the image (excluding the bed elevation, z). The latter is generated through a photogrammetric analysis of stereo images. A challenge arises in combining the maps when the image used to derive the dry surface elevation is at a higher stage than the image used to derive the water depth. This is corrected by applying constant vertical displacement. The resulting RTM is a continuous digital terrain that encompasses the channel bed, floodplains, and the dry terrain features. Qualitative observations of the RTM indicate a correct placement of geomorphic features (pool-riffle system, point bars) for the river. The RTM is used as a model domain for depth-averaged simulations to estimate the bed shear stress corresponding to the formative discharge. The bed material sizes derived from the simulations compare well with field observations. The method presented offers a promising complimentary tool for river analysis.

1 Introduction

In the fields of fluvial sciences, particularly in the ecology department but not limited to, it is often desirable to have a synoptic view of a river in assessing the nature of the system. In the context of sediment transport and channel morphology, a river must be analyzed from the headwaters to the estuary to characterize the sediment caliber distribution, sediment transport rate/capacity, and the resulting channel aggradation/degradation (Church 2002). From an ecology stand point, identification of the major determinants of biota composition, i.e. the sedimentary links (Davey and Lapointe 2007), the various in-stream habitat zones and their longitudinal and lateral connectivity (Bunn and Arthington 2002) require a large-scale understanding of the river.

Despite the need for large-scale assessment of rivers, terrestrial survey methods have been limited in spatial extent. Conventional field surveys (i.e. cross-sectional measurements, sonar, patch sampling) are time consuming, costly, and logistically constrained. In addition, sequential data measurements are prone to error due to the changing environmental variables (imagine making a measurement downstream of a

peaking dam over a day). Consequently, there is considerable difficulty in achieving survey with sufficient spatial extent, spatial density, and frequency of resurvey. (Review of literature show that) There is an increasing trend in supplementing aerial and satellite data to overcome the above-mentioned constraints set by traditional data collection methods.

Since the launch of LANDSAT 1 in 1972, the first of many earth-observing satellites, availability and accessibility to remote sensing data has improved exponentially due to the number of earth-observing satellites launched and the improvements in data storage and transfer technology (J. B. Campbell 2002). Application of remote sensing in aquatic environments initiated in the coastal sciences domain with the primary aim to remotely obtain costal bathymetry. In the past two decades, the river science community has adapted techniques developed for the coastal analysis to drive research in fluvial information extraction from remotely sensed data (i.e. bathymetry, substrate types, turbidity, flow characteristics, in-stream habitat, large woody debris, water temperature). Three major techniques for extracting water depth from remotely sensed data are briefly reviewed.

Physically based technique is based on physics of optics and employ atmospheric and subaquatic radiative transfer models to resolve the components of detected radiance to isolate the bottom-reflected radiance (Bukata 1995). Legleiter et al. (2004) simulated aquatic radiative transfer using the Hydrolight to determine the effect of water depth, substrate type, suspended sediment concentration and turbulence on the bottom reflectance in the Soda Butt-Pebble Creek confluence, US. Legleiter et al. (2009) use the optimal band ratio analysis algorithm and radiative transfer model to retrieve bathymetry for the Soda Butt Creek and the Lamar River, WY, USA at a r^2 of 0.79-0.98. The physically based techniques have shown the capacity to be accurate, yet the complexity of the radiative transfer models seems to deter user. In addition, accuracy and precision of depth estimates vary depending on the channel morphology, thus it is not advisable to rely solely on the technique (Marcus 2012).

Correlation technique employs a regression between the brightness of the image (pixels) and the field depth measurement at the same location to estimate the attenuation coefficient of the water column as a function of depth. It is the simplest of the techniques and most commonly used. Gilvear et al. (1995) correlated field depth measurement to bins of linearly stretched spectral histogram to create a depth map of the Faith River, AK, USA, with a spatial resolution of 1.3m. Winterbottom and Gilvear (1997) used reflectance-measured depth linear function proposed by Lyzenga (1981) for the three bands of the Multi Spectral Scanner (band 5, 6, 8) and aerial panchromatic image to map the depth of the River Tummel, Scotland, with a spatial resolution of 2m and 0.8m and r^2 of 0.67 and 0.55 respectively. Fonstad and Marcus (2005) developed and demonstrated the Hydraulically Assisted Bathymetry model that combined the linear regression of depth-brightness ratio and open channel hydraulics to determine the bathymetry of the Brazos River, TX, USA, with a spatial resolution of 1m and a r^2 of 0.77. Gilvear et al. (2007) regressed field measured reflectance, eliminating the dependence of bottom substrate on the bottom reflectance, and image brightness to obtain a reflectance-depth ratio of the Fourth Estuary, UK, with spatial resolution of 0.66m and r^2 (of the regression) of 0.81-0.87. Lejot et al. (2007) applied the depth-brightness ratio to very high resolution aerial images obtained by paraglider drone to reconstruct the bathymetry of the Rhone River, France with spatial resolution of 14 cm and r^2 of 0.86.

Photogrammetric technique is based on stereoscopy and utilizes a pair of stereo images and stereo matching algorithm (identifying identical ground points on the two images) to reconstruct the water depth. Westaway et al. (2001) used unsupervised stereo matching algorithm of ERDAS Imaging Software with high-resolution aerial photo scans of the North Ashburton River, New Zealand, to retrieve bathymetry with spatial resolution of 37.1 cm and mean errors of 36 cm. Lane et al. (2010) combined photogrammetric technique and depth-brightness modelling in the inundated zones to reconstruct the South Saskatchewan River, Canada, with spatial resolution of 4 cm and mean error of -25 cm-18 cm. Photogrammetric technique requires image resolution in the centimeter ranges, since submerged stereo points can only be match at a spatial resolution fine enough to resolve the texture of the channel bottom. Consequently, such technique often requires custom low flying surveys (i.e. planes and drones), which limit the temporal resolution of the site image (availability of historical records) and increase cost.

In this study, depth-brightness correlation technique was used to reconstruct the water depth map from 0.5 m Geoeye-1 multispectral image. The dry land digital elevation model (DEM) was reconstructed by the vendor using a pair of 0.5 m stereo images from Pleiades-A1. The depth map and the dry land DEM were combined to create a river topography map (RTM), a channel bottom-and-up digital representation of the riverine landscape. As an example of RTM application, digitally reconstructed river was used as a model domain to simulate a bankfull flow in a 2-D hydrodynamic model. Subsequently the simulated bed shear stress was compared against the field sampled sediment caliber in the riffle zone to assess the feasibility of predicting sediment caliber distribution from an image-derived RTM.

In the following, preliminary results of the study is presented. The study site is described in section 2. Next field survey, RTM reconstruction, bankfull discharge estimation and hydrodynamic modelling methodologies are described in section 3. Subsequently, geoprocessing and computational results are presented in section 4. Lastly, conclusion will be drawn in section 5.

2 Study Site

The Goulais River is an eastern tributary of Lake Superior, located 30km north of Salute Ste. Marie, Ontario. It drains an area of approximately 2000 km^2 into the Goulais Bay. It is an unregulated alluvial river, with well-developed meanders for many kilometers upstream of its mouth. The study site is a 13-km reach situated 3.5 km downstream from the township of Searchmont. Its characteristic pool-riffle system is accompanied by alternating point bars and mid channel bars. There are numerous meander cutoffs evident by clearly identifiable oxbow lakes in the satellite images. The floodplain is densely forested with much of the banks covered by tree canopy. During late summer, the site measures as much as 78 cm of flow depth. The channel width ranges between 20 m and 100 m and width transitions occur smoothly.

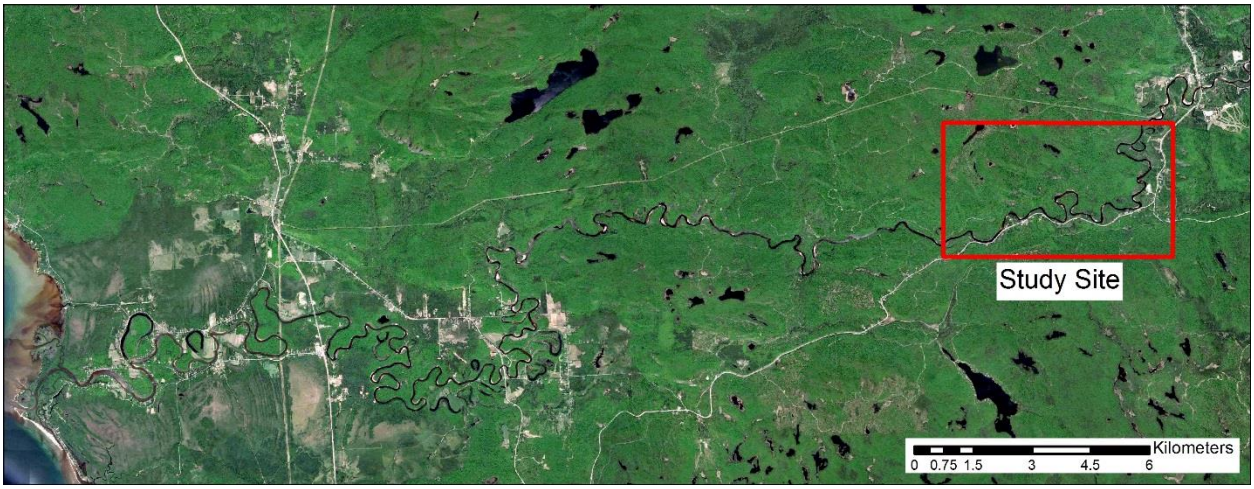

Figure 1. Satellite image of the Goulais River; the river flows from the town of Searchmont (top right), the study site (red box), and drains to the Goulais Bay (bottom left)

3 Methodologies

3.1 Field Measurement

The field survey was conducted by the biologists of Universite de Montreal as a part of the NSERC-HydroNet project on August 14-16, 2011 and July 17-30, 2012. Depth and grain size were measured in 35 rectangular patches (60m x 5m oriented in the streamwise direction).

Depth measurements were collected at 10 different locations for each patch, distributed in a 4 middle- 3 left- 3 right configuration. Grain class distribution was assessed visually at 10 different 50 cm x 50 cm quadrat for each patch, where trained personnel called out the percent grain class based on the Wentworth

grain scale. Median diameter, D_{50}, was measured by collecting medial axial grain width for 50 randomly selected sediments in the patch.

3.2 Depth – band ratio correlation to determine water depth

The image-derived depth map was constructed by a fluvial geomorphology PhD student at McGill University. The 4-band 0.5-m Geoeye-1 satellite image was captured on July 7, 2012 with a discharge of 2.59 m^3/s (hence forth referred to as low flow) measured at the Searchmont gauging station 22km upstream. The field measured depth was regressed against logarithm of band ratio (band 3 [red; 655-690µm] over band 2 [green; 510-580µm]) to yield a linear relationship. The band ratio was chosen to maximize the difference in radiation absorbing properties of water while maintaining adequate penetration to avoid signal saturation (Hugue, et al. 2016). 5 by 5 kernel filter was applied to smooth out the band ratio raster prior to applying the linear relationship to the rest of the submerged pixels. Superficially deep pixels on the shaded side banks were excluded and reinterpolated using minimum curvature spline technique based on 12 neighboring points.

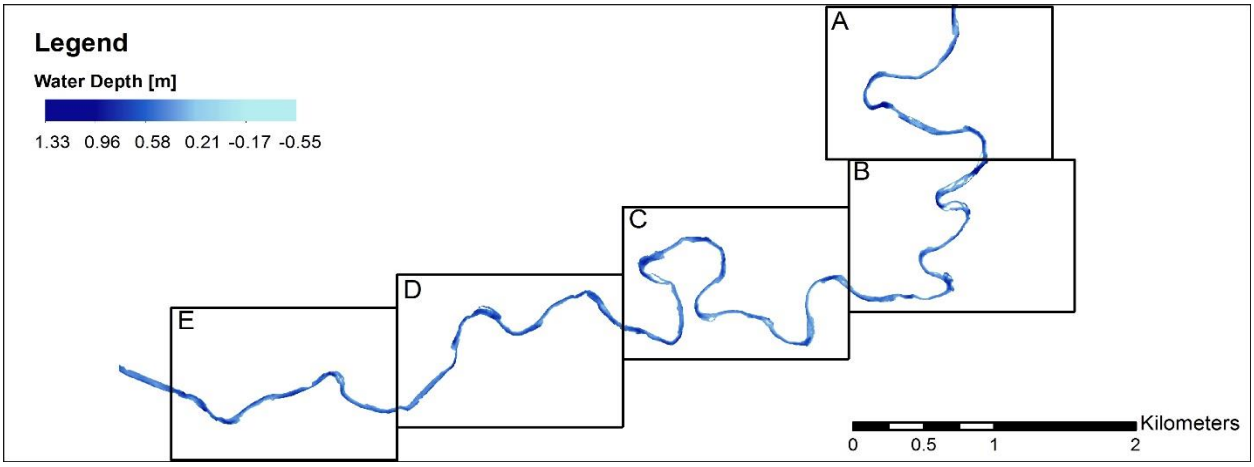

Figure 2. Water depth map of the Goulais River study reach derived from depth – band ratio correlation. The sub-sections shown in Figure 5 are marked. Flow from sub-section A towards E

3.3 Photogrammetry to determine the surface elevation

The 2.5m dry land DEM was reconstructed from 0.5 m stereo images captured by Pleiades-A1. The images were captured on June 14, 2016 with a discharge of 15.01 m3/s (hence forth referred as high flow) measured at the upstream gauging station. The DEM consists of pixel elevations of high flow free surface and the ground topography above it.

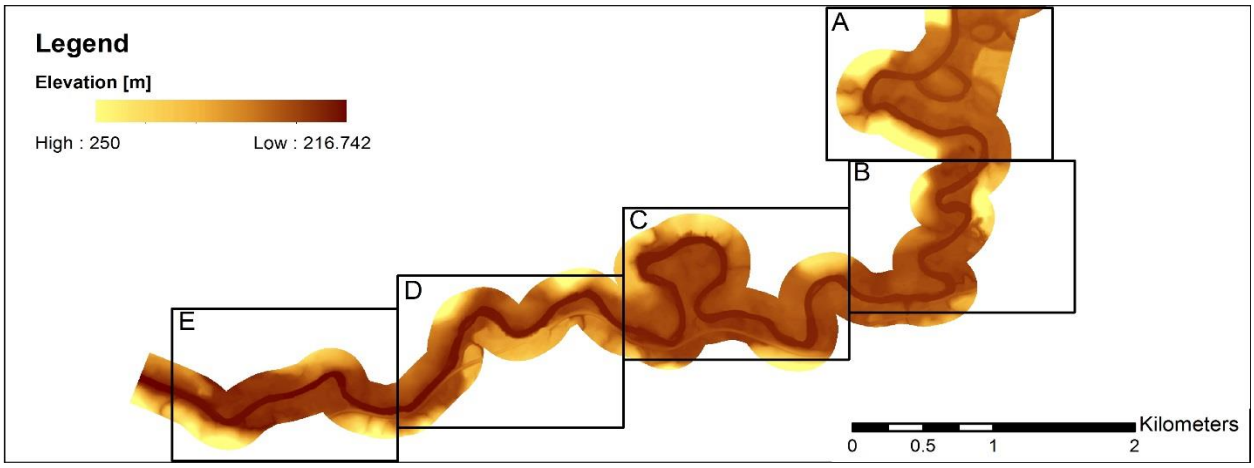

Figure 3. Dry land DEM of the Goulais River study reach derived from photogrammetry. The sub-sections shown in Figure 5 are marked. Flow from sub-section A towards E

3.4 Combining the depth map and the DEM

The water depth map and dry DEM was combined to generate the RTM, which include the submerged channel and the dry land topography. In the process, it has been assumed that no significant channel morphology has taken place between the 4-year gap of the image acquisitions. Here an issue arises due to the mismatched discharge of the images, resulting in a gap, Δh, between the free surfaces that varies in space (streamwise direction).

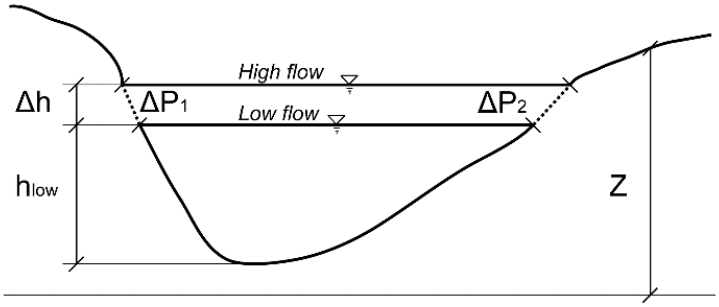

Figure 4. Schematic representation of the missing depth and wetted perimeter between the high flow (dry land DEM) and low flow (water depth map)

Determination of Δh using hydraulic principles has proven to be difficult due to the imperfections in the generated water depth map. In particular, the locust of deepest points in cross sections do not produce a smooth thawleg commonly observed in natural channels. This is mainly due to the persistence of superficially deep sections present in the shaded side banks despite the corrective measure taken. In this study, it was assumed that Δh would have small impact on the eventual bankfull flow simulation results because: 1. For a reach with average channel width of 45 m, the difference in stage between low flow (2.59 m^3/s) and high flow (15.01 m^3/s) should be insignificant; 2. Δh compared to the flow depth at the bankfull discharge (134 m^3/s) should be insignificantly small. Based on the above reasoning, a constant value of 50 cm was applied throughout the reach. The missing wetted perimeter, ΔP, was approximated by discretizing the channel into cross sections at 2 m interval and applying a linear interpolation between the upper edges of low flow and high flow free surfaces.

3.5 Delineation of bankfull depth and bankfull flow

The bankfull discharge was estimated through ensemble of statistical and graphical method. Frequency analysis was conducted on 47-years of peak annual discharge data obtained from the Searchmont gauging station. Peak discharge with a 1.6-year recurrence was determined based on the general consensus of the peak annual discharge of 1-2 year recurrence matching the channel forming bankfull discharge (Petit and Pauquet 1997, Emmett and Wolman 2001, Castro and Jackson 2001).

Subsequently, 9 plots of width-depth ratio against stage was constructed for cross sections in the vicinity of the downstream boundary. The stages of multiple cross sections corresponding to the minimum width-depth ratio was averaged to determine the bankfull stage. Assuming normal flow, the bankfull discharge was determines using the Manning's equation with n=0.0425, Sf=So. The average of the two methods yielded a bankfull discharge of 134 m^3/s.

3.6 Hydrodynamic Simulation

The present study deals with 2D depth-averaged open channel flow. The model equations are solved with finite element solver, Open-TELEMAC 2D.

The depth-averaged model equations are based on the principles of continuity (eq. [1]) and momentum (eq. [2], [3]) as

[1] $$\frac{\partial h}{\partial t} + u_1 \cdot \vec{\nabla}(h) + h div\left(\overrightarrow{u_1}\right) = 0$$

[2] $$\frac{\partial u_i}{\partial t} + \overrightarrow{u_i} \cdot \vec{\nabla}(u_i) = -g \frac{\partial Z}{\partial x_i} + \frac{1}{h} div(h \upsilon_t \vec{\nabla} u_i) + F_i^{\,f}$$

[3] $$F_i^{\,f} = -\frac{u_i}{\cos(\alpha)} \frac{g n^2}{h^{4/3}} \sqrt{u_1^{\,2} + u_2^{\,2}}$$

where subscript $i = 1$ and $i = 2$ denotes the streamwise and lateral component of the variable, h is the flow depth; u is the velocity component; Z is the bed elevation; υ_t is the turbulent eddy viscosity; $F_i^{\,f}$ is the friction force; $\frac{1}{\cos(\alpha)}$ is the norm of the vector normal to the bottom; g is the gravitational acceleration; n is the Manning's roughness coefficient. Depth-averaged $k - \varepsilon$ model was used as turbulence closure. Turbulent viscosity is estimated as a function of turbulent kinetic energy and rate of turbulent dissipation.

Table 1. Summary of hydrodynamics simulation parameters

	Location	Type	Value
Boundary Condition	Inlet	Constant discharge	134 m^3/s
	Outlet	Rating curve[a]	
	Lateral	Free velocity	
	Channel Bottom	Constant Manning's n[b]	0.0425
Initial Condition	Entire Domain	Constant free surface elevation	223 m (1 m/7 m above inlet/outlet)
		Constant velocity	0 m/s
	Inlet	Turbulen quantities gradient	$\frac{\partial k}{\partial h} = 0$, $\frac{\partial \varepsilon}{\partial h} = 0$
Time Step		Constant time step	0.25 s
Simulation Time			5 hrs
CPU Time			25 hrs
Convergence		Minimum residual	< 1E-5

[a] Constructed from low, high and bankfull flow stages. Higher flow stages estimated from normal flow Manning's equation

[b] Based on (Chow, 1959) for major streams with top with at flood stage >100ft

The active channel for the high flow plus a buffer zone of 5 m was discretized with 2 m unstructured mesh (approximately 50 cross channel node count and 2 m along channel interval). In the floodplain, the mesh sized is increased to an edge length of 100m at a growth rate ratio of 1.2 away from the main channel. The details of the simulation are summarized in table 1. By monitoring the 7 cross sectional discharge time series, a steady-state solution was reached at 5 hours simulation time.

3.7 Comparison of simulated bed shear stress and measured sediment caliber

The computed bed shear stress is related to sediment particle diameter based on critical entrainment shear stress for an incipient motion problem. Accordingly, the principles and techniques for rigid-boundary hydraulics are respected. Assuming a homogenous patch, Shield's experiments suggests a nondimensional number (Shield's stress) as

[4] $$\frac{\tau_c}{(\rho_s - \rho)D_s} = \frac{b}{a}$$

where τ_c is the critical shear stress; ρ_s is the sediment density; ρ is the fluid density; D_s is the sediment particle diameter; a is the particle exposure coefficient, b is the static friction coefficient. Shield demonstrated that for gravel and coarser sediments (D_s >5 mm), the Shields stress reaches a constant value of approximately 0.06, suggesting a proportional relationship between critical shear stress and sediment particle diameter. For the smaller sediments, Shield's experimental plot (Shield 1936) was used to graphically extract the corresponding critical shear stress.

4 Results and Discussion

4.1 Reconstructed RTM

In this study the accuracy of the RTM was not verified against detailed field survey due to a lack of available data and resources to carry out a survey of such scale. However, visual inspection of the model conforms with many of the prominent morphological features expected in a meandering river. Series of pool-riffle system can be seen throughout the reach, with a wavelength of approximately 10 channel width. The majority of the thalweg shifts toward the outer bank and high gradient outer bank slopes are observed in the pools. Between two pools, a lateral shift in the location of lowest bed elevation can be observed from one bank to the another, where the centerline is crossed approximately at the intermediary riffle zone. The high gradient side banks of the low flow depth map match with the locations of terraces (remnant of ancient floodplain left behind during the glacial retreat), illustrated by steep banks followed by gently sloping tread.

4.2 Estimation of sediment caliber from shear stress

The sediment caliber in riffle zones were successfully predicted with an r^2 value of 0.90. On the contrary, majority of the predictions in the glides, pools, and runs were overestimated. The author argues that this is the case because the bed shear stress in the riffle zone remain relatively high even at discharge lower than the bankfull discharge. As bankfull discharge events, by definition, occur approximately every 1-2 years, the interim lower flows bring about sediment transport that cause the sediment caliber distribution to deviate from the distribution just after the bankfull event. This effect is most prominent in the pools, and to a lesser degree in the proximal and distal ends, due to the reduced velocity (reduced bed shear stress) during low flows, leading to vertical accretion of finer sediments (sand and silt). This causes the previously mobilized larger sediments during the bankfull event to be covered by the finer sediments. In addition, one to one relationship is not expected to hold between sediment caliber and bankfull shear stress in the non-riffle zone due to the complex 3-D flow patterns of helicoidal flow, which cannot be accounted for in 2-D simulation. The cork-screw like secondary flow acts as a mechanism to sort sediments in the lateral plane.

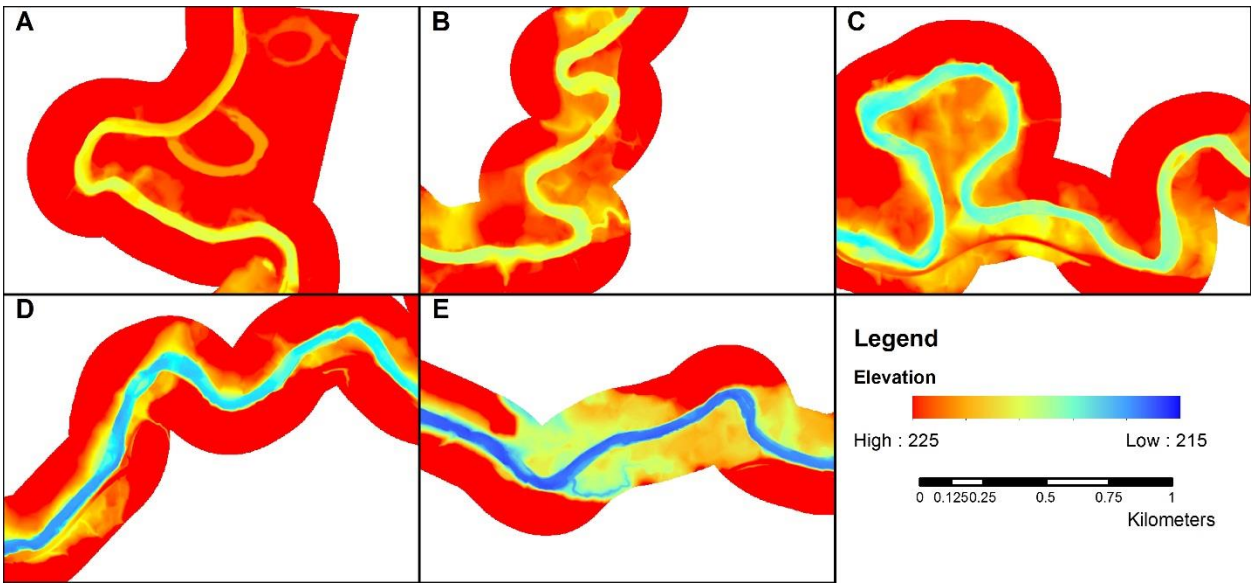

Figure 5. River terrain model of sub-sections of the Goulais River study site

The underprediction of the sediment caliber is most likely due to misrepresentation of colluvium (sediments transported to a location independent of the river flow, i.e. rainwash, sediments falling from side banks, etc.) as alluvium (sediments transported to a location by fluvial transport) during the field survey. Colluvium is supply limited, meaning its loading on the river is independent of the hydrodynamics of the river. Since the biologists did not discern the two types of sediments, it is hard to conclude with certainty. For the underestimated patches in the left bank, particularly in those situated adjacent to the road, measurements may have coincided with locations of riprap, where larger boulders were introduced artificially to prevent lateral erosion.

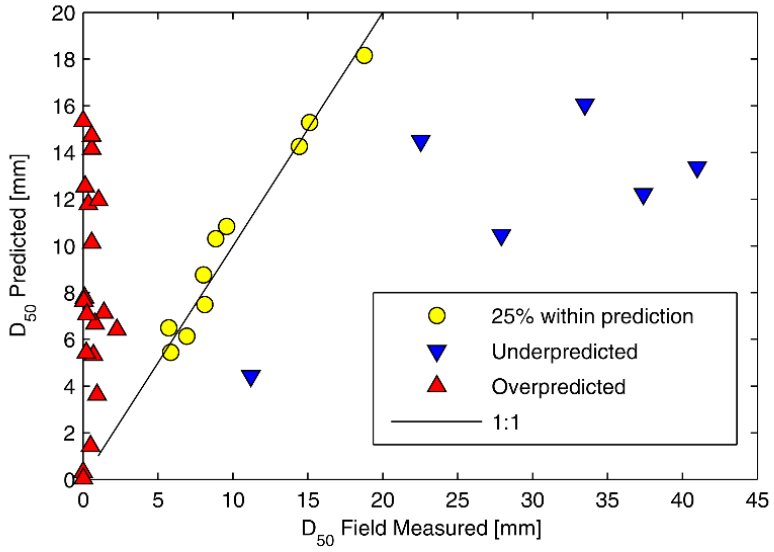

Figure 6. Comparison of field measured and predicted sediment caliber

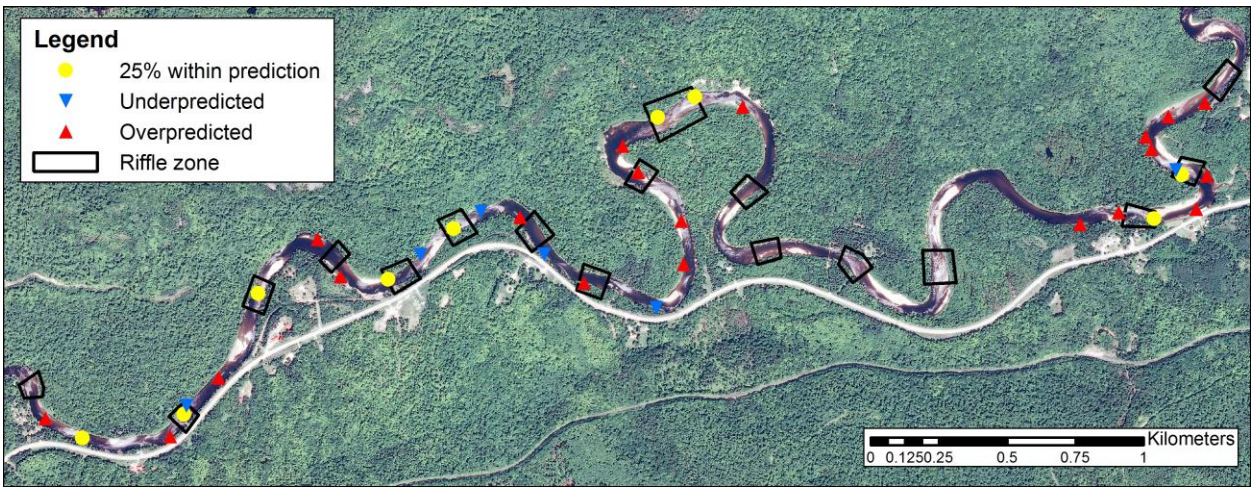

Figure 7. Spatial representation of the prediction performance

5 Conclusion

This paper reports digital reconstruction of channel bed, floodplain and dry land topography using minimal field measurement and multispectral and stereo pair satellite imagery. Depth-band ratio (red/green) regression was used to estimate the bathymetry from the image pixels. The depth map and the dry land DEM was combine with an addition of constant depth discrepancy to account for the difference in discharges. The RTM was used as a model domain to simulate a bankull flow event in a 2D hydrodynamic model. The following conclusions have been reached:

- The simulated bed shear stresses in the riffle zones showed strong positive correlation with the field measured sediment caliber. The bed shear stress in the riffle zone is large enough during the interim low flow seasons to maintain the sediment distribution to be comparable to that of immediately after a bankfull event.
- The wellness of correlation between the predicted and measured sediment caliber confirms that, in a bankfull event study, the choice of depth discrepancy between the low and high flows is insensitive to the resulting shear stress distribution.
- Overprediction of sediment caliber in the pools and their neighbors suggests the necessity for more sophisticated technique to account for the complex hydrodynamics and the multi-dimensional interactions of the sediments and the flow.

Acknowledgement

Financial support from National Sciences and Engineering Research Council of Canada through Discovery Grant held by S. Li is acknowledged.

References

Bukata, R. P. 1995. "Optical Properties and Remote Sensing of Inland and Coastal Waters." 54. Boca Raton, FL: CRC Press.

Bunn, S., and A. Arthington. 2002. "Basic principles and ecological consequences of altered flow regimes for aquatic biodiversity." Environmental Management 492-507.

Campbell, J. B. 2002. Introduction to Remote Sensing. New York: Gilford Press.

Campbell, J. 2002. "Introduction to Remote Sensing." 46-48. New York: Guilford Press.

Castro, J. M., and P. L. Jackson. 2001. "Bankfull discharge reccurence intervals and regional hydraulic geometry relationships: patters in the Pacific Northwest, USA." Journal of American Water Resources Assiciation 1249-1262.

Church, M. 2002. "Geomorphic thresholds in riverinee landscapes." Freshwater Biology 541-557.
Davey, C., and M. Lapointe. 2007. "Sedimentary links and stapial organization of Atlantic salmon (Salmo salar) spawmomg habitat in a Canadian Shield river." Geomorphology 82-96.
Emmett, W. W., and M. G. Wolman. 2001. "Effective discharge and gravel-bed rivers." Earth Surface Processes and Landforms 1369-1380.
Fonstad, M. A., and W. A. Marcus. 2005. "Remotesensing of stream depths with hydraulically assisted bathymetry (HAB) models." Geomorphology 320-339.
Gilvear, D. J., P. Hunter, and T. Higgins. 2007. "An experimental approach to the measurement of the effect of water depth and substrate on optical and near infra-red reflectance: a field-based assessment of the feasibility of mapping submerged instream habitat." International Journal of Remote Sensing 2241-2256.
Gilvear, D. J., T. M. Waters, and A. M. Milner. 1995. "Image analysis of aerial photograph to quantiify changes in channel morphology and instream habitat following placer mining in interior Alaska." Freshwater Biology 389-398.
Hugue, F., M. Lapointe, B. C. Eaton, and A. Lepoutre. 2016. "Satellite-based remote sensing of running water habitats at large riverscape." Geomorphology 353-369.
Lane, S. N., P. E. Widdison, R. E. Thomas, P. J. Ashworth, J. L. Best, I. A. Lunt, G. H. Samrook Smith, and C. J. Simpson. 2010. "Quantification of braided river channel change using archival digital image analysis." Earth Surface Processes and Landforms.
Legleiter, C. J., D. A. Roberts, and R. L. Lawrence. 2009. "Spectrally based remote sensing of river bathymetry." Earth Surface Processes and Landforms 1039-1059.
Legleiter, C. J., D. A. Roberts, W. A. Marcus, and M. A. Fonstad. 2004. "Passive optical remote sesing of river channel morphology and in-stream habitat: Physical basis and feasibility." Remote Sensing of Environment 493-510.
Lyzenga, D. R. 1981. "Remote sensing of bottom reflecrance and water attenuation parameters in shallow water using aircraft and LANDSAD data." International Journal of Remote Sensing 71-82.
Marcus, W. A. 2012. "Remote sensing of hydraulic environment in grave-bed rivers." In Gravel-bed Rivers: Processes, Tools, Environments, by M. Church, B. M. Pasccak and A. G. Roy, 269. Singapore: Wiley-Blackwell.
Petit, F., and A. Pauquet. 1997. "Bankfull discharge reccurence interval in gravel-bed rivers." Earth Surface Processes and Landforms 685-693.
Shield, A. 1936. "Application of similarity principles and turbulence research to bed-load movement." Hydrodynamics Laboratory publication.
Westaway, R. M., S. N. Lane, and D. M. Hick. 2001. "Remote sensing of clear-water, shallow, grave-bed rivers using digital photogrammetry." Photogrammetric Engineering & Remote Sensing 1271-1281.
Winterbottom, S. J., and D. J. Gilvear. 1997. "Quantification of channel bed morphology in gravel-bed rivers using airborne multispectral imagery and aerial photograph." Regulated Rivers: Research & Management 489-499.